

## Resolvent-based feedback control of vortex shedding at low Reynolds numbers

B. Jin, R. D. Sandberg and S. J. Illingworth

Department of Mechanical Engineering  
 The University of Melbourne, Victoria 3010, Australia

### Abstract

Feedback control of vortex shedding behind a 2D cylinder at low Reynolds numbers is investigated using a resolvent approach. This work presents an efficient modelling approach by capturing the input-output dynamics of an incompressible flow from the resolvent operator (i.e. the frequency response) of the linearized Navier-Stokes equations. The difficulty of applying modern control design techniques to complex, high-dimensional flow systems is overcome by exploiting low-order models identified from frequency responses. We design optimal control laws by applying  $H_\infty$  loop shaping to the low-order models for a range of Reynolds numbers. Two single-input single-output control arrangements are examined. The first setup is a velocity measurement in the cylinder wake to drive a pair of body forces located near the separation points. Complete suppression of shedding is observed up to  $Re = 110$ . We also observe a fundamental trade-off: the sensor should be close enough to the cylinder to reduce the excessive time lag, but it should be kept sufficiently far from the cylinder to measure unstable eigenmodes developed downstream. These two conflicting requirements become more difficult to satisfy for larger Reynolds numbers. The second setup utilises cylinder lift measurement to oscillate the cylinder. We observe that control for this arrangement is more challenging, with complete suppression of vortex shedding achieved only up to  $Re = 60$ . The reasons for the difficulty of control for these two control arrangements are discussed.

### Introduction

The flow around a bluff body becomes unstable above the critical Reynolds number and results in alternate vortex-shedding. It gives rise to strong force fluctuations which are responsible for structural vibrations, acoustic noise and resonance. Many efforts have been made to suppress vortex shedding [2, 9]. In the past, passive control has received considerable attention due to the simplicity of its practical implementation. A simple modification of the geometry or structural additions can be used to affect the flow beneficially. Another way to alter a flow is introducing powered actuators and injecting energy in a sensible way. This is called active open-loop control, which operates according to pre-defined laws and shows poor robustness.

A more robust and efficient way to control the flow is active closed-loop control or feedback control, which comprises actuators operating according to the feedback signals provided by sensors. Unexpected disturbances or uncertainties in the flow are compensated, which leads to better control performance and robustness than that achieved using the passive or active open-loop control. In this paper, we focus our attention on reducing the vortex shedding behind a 2D circular cylinder using feedback control. Control design for such flows requires special care due to the high-dimensionality and non-linearity of the Navier-Stokes equations. Many control design techniques based on control theory are too computationally expensive to be applied to the full Navier-Stokes equations.

Many attempts have been made to simplify flow systems includ-

ing reduced order models (ROMs) which approximate flow dynamics and make the problem computationally tractable. This paper presents an efficient modelling approach based on the resolvent operator of the linearized Navier-Stokes equations. The method effectively captures linear input-output dynamics of the flow without using numerical simulation data or experimental data. The effectiveness of the resulting models is shown by designing robust stabilising feedback controllers for two control arrangements.

### Linear modelling approach

#### Transfer function of linear flow dynamics

The objective of feedback control is to completely suppress the vortex shedding behind a 2D circular cylinder. In other words, we attempt to drive the flow towards its unstable steady state (base flow), around which the Navier-Stokes equations are linearized. The following formalism mainly follows the work of Sipp et al. [9]. To investigate the dynamics of incompressible flow near its steady state, we perform an input-output analysis of the forced Navier-Stokes equations:

$$\frac{\partial \mathbf{u}}{\partial t} + \mathbf{u} \cdot \nabla \mathbf{u} = -\nabla p + \nu \nabla^2 \mathbf{u} + \mathbf{f}', \quad \nabla \cdot \mathbf{u} = 0, \quad (1)$$

where the source term  $\mathbf{f}'$  in the momentum equations models the external forcing with zero steady term. The governing equations of the linear flow dynamics around the base flow  $(\mathbf{U}, P)$  are

$$\frac{\partial \mathbf{u}'}{\partial t} + \mathbf{U} \cdot \nabla \mathbf{u}' + \mathbf{u}' \cdot \nabla \mathbf{U} = -\nabla p' + \nu \nabla^2 \mathbf{u}' + \mathbf{f}', \quad \nabla \cdot \mathbf{u}' = 0. \quad (2)$$

Here,  $(\mathbf{u}', p')$  represents the unsteady component, the small perturbation around the steady state.  $\nabla$  is defined as  $(\partial/\partial x, \partial/\partial y)$  and  $\nu$  is the kinematic viscosity. The nonlinear term  $\mathbf{u}' \cdot \nabla \mathbf{u}'$  can be neglected following an assumption of small perturbations. To evaluate the linear dynamics of a flow system, it is convenient to take Laplace transforms. Introducing the transformation into equation (2), we obtain the equations

$$s\hat{\mathbf{u}} + \mathbf{U} \cdot \nabla \hat{\mathbf{u}} + \hat{\mathbf{u}} \cdot \nabla \mathbf{U} = -\nabla \hat{p} + \nu \nabla^2 \hat{\mathbf{u}} + \hat{\mathbf{f}}, \quad \nabla \cdot \hat{\mathbf{u}} = 0, \quad (3)$$

where  $(\hat{\mathbf{u}}, \hat{p})$  and  $\hat{\mathbf{f}}$  represent the complex spatial structure of the response and forcing waves respectively and  $s = \sigma + j\omega$  is the Laplace variable. Thus, the transfer function between the external forcing and response can be written as

$$\begin{bmatrix} \hat{\mathbf{u}} \\ \hat{p} \end{bmatrix} = (s\mathcal{E} - \mathcal{A})^{-1} \begin{bmatrix} \hat{\mathbf{f}} \\ 0 \end{bmatrix}, \quad (4)$$

where  $(s\mathcal{E} - \mathcal{A})^{-1}$  is known as the resolvent operator.  $\mathcal{A}$  is the linearized Navier-Stokes operator around the base flow

$$\mathcal{A} = \begin{bmatrix} -\mathbf{U} \cdot \nabla - (\cdot) \cdot \nabla \mathbf{U} + \nu \nabla^2 & -\nabla \\ \nabla \cdot (\cdot) & 0 \end{bmatrix}, \quad \mathcal{E} = \begin{bmatrix} I & 0 \\ 0 & 0 \end{bmatrix}. \quad (5)$$

Consider writing equation (5) in state-space form for a linear, time-variant dynamical system  $P(s)$ :

$$\begin{aligned} s\mathcal{E}\mathbf{x} &= \mathcal{A}\mathbf{x} + \mathcal{B}e \\ \mathbf{y} &= \mathcal{C}\mathbf{x} + \mathcal{D}e, \end{aligned} \quad (6)$$

where  $\mathbf{x} = [\hat{\mathbf{u}} \ \hat{p}]^T$  is the system state,  $e$  is an input vector of

dimension  $p$  and  $y$  is an output vector of dimension  $q$ . The feedback control arrangement used here is single-input single-output (SISO) with  $p = q = 1$ . The vector  $\mathcal{B}$  is determined by the shape of the actuation, which is from the spatial discretization of the external forcing term  $\hat{f}$ . The matrices  $\mathcal{C}$  and  $\mathcal{D}$  represent output and feed-forward dynamics respectively. The transfer function between the output and input can be written as

$$P(s) = \mathcal{C}(s\mathcal{E} - \mathcal{A})^{-1}\mathcal{B} + \mathcal{D}. \quad (7)$$

In general  $P(s)$  is of high dimension, which makes the control design problem computationally intractable. However, it still provides input-output data which can be used to form reduced order models using vector-fitting algorithm VECTFIT [4]. VECTFIT identifies a reduced-order model  $\tilde{P}(s)$  of a significantly smaller dimension  $N$  which has almost the same response as the original system  $P(s)$  for harmonic input ( $s = j\omega$ ) within a broad frequency range.

### Numerical flow solver

We consider an incompressible flow past a 2D circular cylinder of diameter  $D$ . The Reynolds number is defined as  $Re = U_\infty D/\nu$  where  $U_\infty$  is the free-stream velocity. The computational domain is the same as the domain used by Leontini et al. [6]. The mesh consists of  $5.46 \times 10^4$  triangles and their wall-normal size around the cylinder is 0.01. The discretization is supported by the computing platform FEniCS [7] with Taylor-Hood finite elements in space and backward Euler scheme in time ( $\Delta t = 0.01$ ). Two control setups are considered as shown in figure 1. In the first case, a uniform free-stream velocity ( $U_\infty = 1, V_\infty = 0$ ) is imposed at the inlet boundary and encounters a stationary cylinder located at  $(x = 0, y = 0)$  where no-slip boundary conditions are enforced. Symmetric boundary conditions ( $\partial u/\partial y = 0, v = 0$ ) are applied on the top and bottom boundaries ( $0 < x < 23, y = \pm 15$ ). Standard outflow boundary conditions are used at the outlet boundary ( $x = 23, -15 < y < 15$ ):  $-pn + \nu \nabla \mathbf{u} \cdot \mathbf{n} = 0$ , where  $\mathbf{n}$  denotes the outward-pointing normal vector on the boundary. In the second control arrangement, instead of moving the cylinder directly, the flow is solved in an accelerated frame of reference attached to the cylinder. To allow this, the cylinder acceleration  $\hat{a}$  is treated as an extra forcing term  $\hat{f}$  and the boundary conditions are modified accordingly. More details can be found in Leontini et al. [6].

The base flow ( $U, P$ ), which is governed by the unforced steady Navier–Stokes equations, is solved using a Newton method. The boundary conditions for the base flow are the same as those described above. The perturbation flow field ( $\hat{u}, \hat{p}$ ) has similar boundary conditions except at the inlet where homogeneous boundary conditions are enforced ( $\hat{u}_\infty = 0$ ) to ensure zero perturbations at infinity. The stability analysis of the base flows and perturbation systems have been validated using the results of Barkley [1]. To validate the controllers, direct numerical simulations are performed using the IPCS (Incremental Pressure Correction Scheme) method which is extensively tested [7].

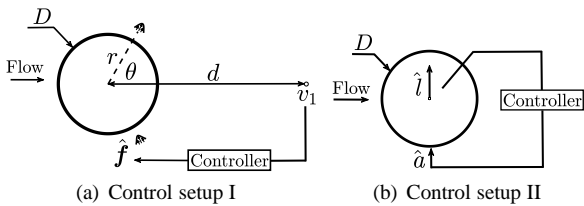


Figure 1: **(a)** A pair of body forces applied near cylinder surface cooperates with a velocity sensor placed on the centreline with a distance  $d$  from the center of the cylinder. **(b)** The force sensor is placed on the cylinder to measure the lift which is fed to the actuator that controls the acceleration of the cylinder.

## Resolvent-based feedback control

### Actuator and sensor setup

Two control setups are considered which are shown in figure 1. In-flow and body-mounted sensors and actuators are utilised to compare their potential performances. Control setup I uses a pair of anti-symmetrical body force  $\hat{f}$  as the source term defined in equation 3 for actuation and the velocity in the wake for sensing. Such arrangement is suitable for the analysis of sensor or actuator placement. The centers of two actuation regions are at a distance of  $r = 0.6$  from the cylinder's center and at an angle of  $\theta = \pm 70^\circ$  from the cylinder's downstream-pointing horizontal. The basic distribution of each actuation region is Gaussian governed by

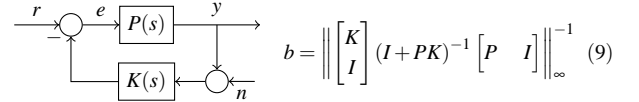
$$S(A, r, \theta, \sigma) = \frac{A}{2\pi\sigma^2} \exp\left(-\frac{(x-x_0)^2 + (y-y_0)^2}{2\sigma^2}\right). \quad (8)$$

where  $A = 1.0$  and  $\sigma = 0.1$ . Moreover, the center of the actuation is defined by  $x_0 = r\cos(\theta)$  and  $y_0 = r\sin(\theta)$ . The actuator parameters are chosen such that the body force should be concentrated near the separation points to affect the vortex shedding. The sensor is positioned a distance  $d$  downstream of the cylinder and measures transverse velocity  $v_1$ . This arrangement is similar to that used in Illingworth [5].

Control setup II is a more practical arrangement as shown in figure 1(b). Actuation is provided by oscillation of the cylinder and its transverse acceleration  $\hat{a}$  is actuated. The feedback signal is provided by a force sensor attached to the cylinder which measures the lift  $\hat{l}$ . Thus, both actuator and sensor are placed on the cylinder without any necessity to consider their placements.

### $H_\infty$ optimal control

The feedback controller is designed based on the reduced-order model  $\tilde{P}(s)$  using  $H_\infty$  loop-shaping. The feedback arrangement considered is shown below.



where  $b \in [0, 1]$ ,  $r$  is disturbances at the input and  $n$  represents noise at the sensor. The controller  $K(s)$  for plant  $P(s)$  is designed using the loop shaping design method by Glover-McFarlane [3] which maximizes the normalized coprime stability margin  $b(P, K)$  of plant-controller feedback loop. Physically, it's an indication of the robustness of the closed-loop system to unmodelled dynamics and used as a performance measure here. For SISO systems as considered here, a compensator which weights the plant according to the control objectives is in the same form as the weight used by Illingworth [5]. The form of the control weight is

$$W(s) = k \frac{a^2}{(s+a)^2}. \quad (10)$$

with parameters  $k$  and  $a$  to be chosen.

## Results

### Simulated cases and model reduction

The Reynolds number considered in this paper ranges from  $Re = 40$  to 110 for control setup I and from  $Re = 40$  to 100 for setup II. In both cases, the sensor location and the weight parameters are chosen after searching different value combinations to ensure the largest optimal stability margin  $b_{opt}$ .

Before the reduced-order models are used for control design, they should first be validated. The order of ROMs is chosen such that the fitting residual is below  $1 \times 10^{-5}$ . This is achieved with a model order of 30 or less for all  $Re$  considered. Results at Reynolds number of 60 are shown in figure 2. Figure 2(a) shows the frequency responses of the flow systems  $P(j\omega)$  and the ROMs for control setup I and II respectively. The corresponding gains and phases are almost identical. The comparisons of open-loop impulse responses (with magnitude  $1 \times 10^{-4}$ ) between the original systems and ROMs show excellent agreement in figure 2(b). Thus, the reduced-order models we found are good approximations of the true systems.

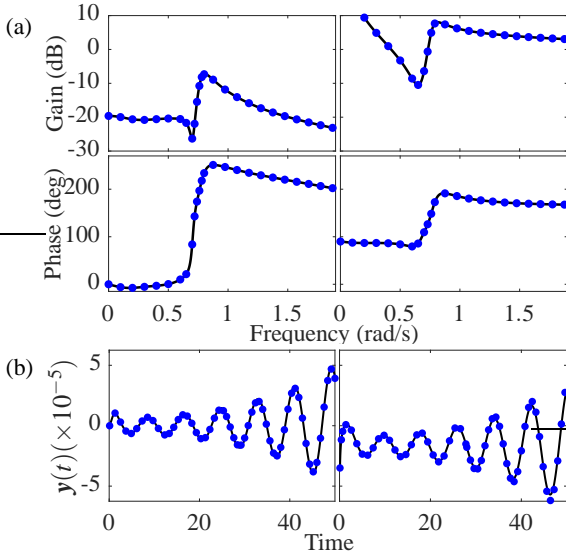


Figure 2: (a) Frequency responses from  $P(j\omega)$  (—) compared to those from the ROMs (•) for control setup I (left) and setup II (right) at  $Re = 60$ . (b) The corresponding open-loop impulse responses from numerical simulations. The results for setup II are multiplied by 0.25 so that the same scale can be used.

### Feedback control of vortex shedding

The feedback controllers are designed based on the ROMs using  $H_\infty$  loop shaping. The optimal stability margin  $b_{opt}$  is shown in figure 3 for two control setups at different Reynolds numbers and for different sensor locations. Figure 3(a) indicates that the largest optimal stability margin  $b_{opt}$  (best performance and robustness achieved) for each control setup is decreasing sharply with increasing Reynolds number. We also see that control setup I provides larger  $b_{opt}$  for all the Reynolds numbers considered. A contour map of  $b_{opt}$  for control setup I is plotted against Reynolds number and sensor location  $d$  in figure 3(b). The dashed line represents the optimal sensor location as a function of Reynolds number. A fundamental trade-off is observed: the sensor should be close enough to the cylinder to reduce the time delay due to convection but it should also be far enough from the cylinder to measure the information (e.g. unstable eigenmodes) developed in the downstream. The compromise between these two conflict requirements becomes harder to satisfy with increasing Reynolds number, which leads the optimal sensor location moving downstream linearly. Similar results are observed in recent work [8] which considers feedback control of the linearized Ginzburg-Landau system.

All control laws are validated in DNS by testing closed-loop impulse responses (with magnitude  $1 \times 10^{-2}$ ). For each control setup, results at two representative Reynolds numbers are plotted in figure 4. The top row in the figure represents control setup I, where the optimal feedback controller designed for

$Re = 60$  is compared to the controller designed for  $Re = 110$ . The first thing to note is that the vortex shedding is completely suppressed for both Reynolds numbers as shown by transverse velocity  $v_1(t)$  at the sensor and total perturbation energy  $E(t)$  (figure 4(b)). It is also obvious that the controller at  $Re = 60$  performs much better as shown in the simultaneous vorticity perturbation fields (figure 4(c)) at the two Reynolds numbers. The same quantities for control setup II are also shown in figure 4(e,f) but at  $Re = 60$  and  $Re = 80$ . Even though feedback control laws suppress the vortex shedding for all cases, the controller designed for  $Re = 80$  shows poorer performance. From the comparison among all four cases, we can see that vortex shedding is harder to suppress at higher Reynolds numbers. More importantly, control setup I performs significantly better than setup II at the same Reynolds number. These conclusions are consistent with the values of  $b_{opt}$  as shown in figure 3: the higher the optimal stability margin  $b_{opt}$  is, the better the feedback controller performs.

The poor feedback performance and small stability margins can be linked to the roots of the relevant transfer functions. Figure 4(a,d) shows right-half plane (RHP) zeros of ROMs near unstable poles for these cases. The comparison between the two control setups at  $Re = 60$  ( $\times/\circ$ ) indicates that the transfer function of setup II has an extra pair of RHP zeros. The existence of RHP zeros is problematic for control design because they limit the bandwidth that can be controlled with good performance and robustness. Therefore, RHP zeros near the unstable poles severely restrict the performance and robustness, which are measured by  $b_{opt}$ . A physical interpretation is that the unstable eigenmodes required to be controlled develop downstream, which appear only weakly at the sensor location. Therefore RHP zeros here imply that the unstable modes are nearly invisible to the sensor. Increasing Reynolds number also moves the zeros to the RHP, which can be seen from the comparison between black markers ( $\times/\circ$ ) and blue markers ( $\times/\bullet$ ) in figure 4(a) or (d). The RHP zeros for control setup I at  $Re = 110$  is actually caused by the time delay from convection because the sensor has been moved from  $d = 1.13$  to  $d = 3.43$ . The sensor measures outdated information which is fed to the controller. However, when the sensor is placed at the same location as the actuator, as for control setup II, increasing Reynolds number makes unstable eigenmodes more invisible to the sensor because they become weaker near the cylinder at a higher Reynolds number.

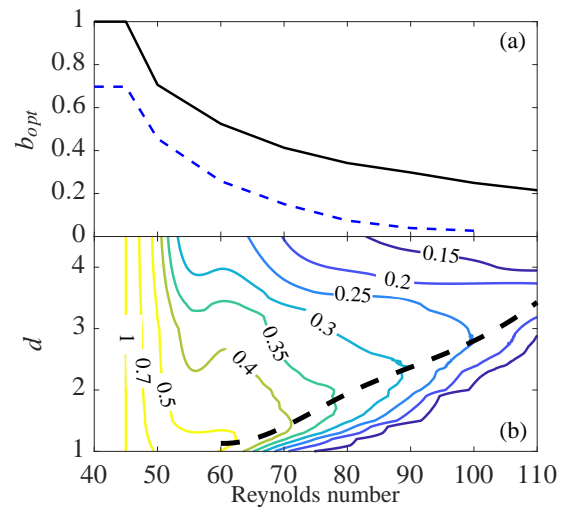


Figure 3: (a) Largest optimal stability margin  $b_{opt}$  at different Reynolds numbers for control setup I (—) and setup II (---). (b) Optimal sensor locations (---) and contour plot of  $b_{opt}$  for control setup I against Reynolds number and sensor location  $d$ .

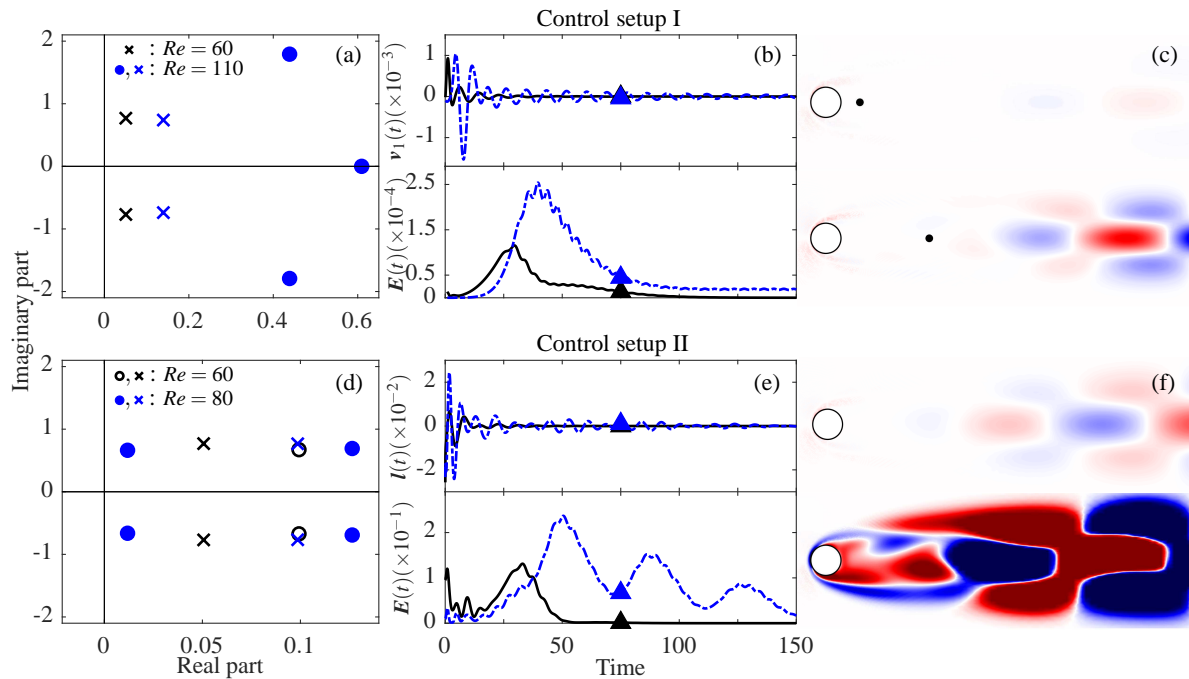


Figure 4: (Top row) Control setup I. (a) RHP zeros ( $\circ/\bullet$ ) of reduced order models near unstable poles ( $\times/\times$ ) at two Reynolds numbers. (b) The transverse velocity (top) at the sensor ( $\bullet$  in c) and the total perturbation energy (bottom) at  $Re = 60$  (—) and  $Re = 110$  (---). The energy for  $Re = 110$  is multiplied by 0.01 so that the same scale can be used. (c) Spatial maps of vorticity perturbation at  $t = 75$  ( $\blacktriangle/\blacktriangle$ ) for  $Re = 60$  (top) and  $Re = 110$  (bottom). (Bottom row) Control setup II. (d, e, f) have the same layout as (a, b, c) at  $Re = 60$  and  $Re = 80$ . The energy for  $Re = 80$  is multiplied by 0.1 so that the same scale can be used. All contour plots have the same scale  $\pm 0.05$ .

## Conclusions

We use a system identification method to model the 2D linearized cylinder flow from its resolvent operator, then design controllers for reduced-order models using a  $H_\infty$  method. ROMs are identified from the actual frequency responses of linearized flow systems and validated in DNS by comparing their impulse responses. The controllers are validated by applying them to the original high-order systems. We investigate two single-input single-output control setups and successfully suppress the vortex shedding at the Reynolds numbers considered.

The sensor placement is crucial to the performance and robustness of the controller. The control setup with oscillatory cylinder attached by a force sensor shows poorer performance than the in-flow sensor setup at all Reynolds numbers considered. Such control setup has the same sensor and actuator position, which implies that the unstable eigenmodes developed downstream cannot be sufficiently well captured. This limitation manifests itself in the form of RHP zeros near the unstable poles in the root maps of the ROMs. Different sensor positions are examined for the in-flow sensor setup to further investigate the roles of sensor placement. The corresponding optimal sensor locations indicate two principles of the sensor placement: on the one hand, it should be close enough to the actuator to receive the information in a timely fashion; on the other hand, the sensor is required to measure unstable eigenmodes developed in the downstream. Difficulties in satisfying these two conflicting requirements cause a deterioration of the optimal controller's performance and robustness.

The present work validated an efficient modelling approach which doesn't require any DNS or experimental data. The method supports a preliminary investigation of the role of sensor placement in the 2D cylinder flow. The observation of a fundamental trade-off when choosing the optimal sensor location provides important guidance for further research in optimal sensor and actuator selection.

## References

- [1] Barkley, D., Linear analysis of the cylinder wake mean flow, *EPL (Europhysics Letters)*, **75**, 2006, 750.
- [2] Choi, H., Jeon, W.-P. and Kim, J., Control of flow over a bluff body, *Annu. Rev. Fluid Mech.*, **40**, 2008, 113–139.
- [3] Glover, K. and McFarlane, D., Robust stabilization of normalized coprime factor plant descriptions with h/sub infinity/-bounded uncertainty, *IEEE transactions on automatic control*, **34**, 1989, 821–830.
- [4] Gustavsen, B. and Semlyen, A., Rational approximation of frequency domain responses by vector fitting, *IEEE Transactions on power delivery*, **14**, 1999, 1052–1061.
- [5] Illingworth, S. J., Model-based control of vortex shedding at low Reynolds numbers, *Theoretical and Computational Fluid Dynamics*, **30**, 2016, 429–448.
- [6] Leontini, J., Stewart, B., Thompson, M. and Hourigan, K., Wake state and energy transitions of an oscillating cylinder at low Reynolds number, *Physics of Fluids*, **18**, 2006, 067101.
- [7] Logg, A., Mardal, K.-A. and Wells, G., *Automated solution of differential equations by the finite element method: The FEniCS book*, volume 84, Springer Science & Business Media, 2012.
- [8] Oehler, S. F. and Illingworth, S. J., Sensor and actuator placement trade-offs for a linear model of spatially developing flows, *J. Fluid Mech.*, **Accepted July 2018**.
- [9] Sipp, D., Marquet, O., Meliga, P. and Barbagallo, A., Dynamics and control of global instabilities in open-flows: a linearized approach, *Applied Mechanics Reviews*, **63**, 2010, 030801.